IpdAB, a virulence factor in *Mycobacterium tuberculosis*, is a cholesterol ring-cleaving hydrolase

Adam M. Crowe[a], Sean D. Workman[a,b], Nobuhiko Watanabe[a,b], Liam J. Worrall[a,b], Natalie C. J. Strynadka[a,b], and Lindsay D. Eltis[a,c,1]

[a]Department of Biochemistry and Molecular Biology, Life Sciences Institute, The University of British Columbia, Vancouver, BC, Canada, V6T 1Z3; [b]The Center for Blood Research, Life Sciences Institute, The University of British Columbia, Vancouver, BC, Canada, V6T 1Z3; and [c]Department of Microbiology and Immunology, Life Sciences Institute, The University of British Columbia, Vancouver, BC, Canada, V6T 1Z3

Edited by William R. Jacobs Jr., HHMI and Albert Einstein College of Medicine, Bronx, NY, and approved February 23, 2018 (received for review October 2, 2017)

***Mycobacterium tuberculosis* (*Mtb*) grows on host-derived cholesterol during infection. IpdAB, found in all steroid-degrading bacteria and a determinant of pathogenicity, has been implicated in the hydrolysis of the last steroid ring. Phylogenetic analyses revealed that IpdAB orthologs form a clade of CoA transferases (CoTs). In a coupled assay with a thiolase, IpdAB transformed the cholesterol catabolite (*R*)-2-(2-carboxyethyl)-3-methyl-6-oxocyclohex-1-ene-1-carboxyl-CoA (COCHEA-CoA) and CoASH to 4-methyl-5-oxo-octanedioyl-CoA (MOODA-CoA) and acetyl-CoA with high specificity (k_{cat}/K_m = 5.8 ± 0.8 × 10^4 $M^{-1}·s^{-1}$). The structure of MOODA-CoA was consistent with IpdAB hydrolyzing COCHEA-CoA to a β-keto-thioester, a thiolase substrate. Contrary to characterized CoTs, IpdAB exhibited no activity toward small CoA thioesters. Further, IpdAB lacks the catalytic glutamate residue that is conserved in the β-subunit of characterized CoTs and a glutamyl-CoA intermediate was not trapped during turnover. By contrast, $Glu105^A$, conserved in the α-subunit of IpdAB, was essential for catalysis. A crystal structure of the IpdAB·COCHEA-CoA complex, solved to 1.4 Å, revealed that $Glu105^A$ is positioned to act as a catalytic base. Upon titration with COCHEA-CoA, the $E105A^A$ variant accumulated a yellow-colored species (λ_{max} = 310 nm; K_d = 0.4 ± 0.2 μM) typical of β-keto enolates. In the presence of D_2O, IpdAB catalyzed the deuteration of COCHEA-CoA adjacent to the hydroxylation site at rates consistent with k_{cat}. Based on these data and additional IpdAB variants, we propose a retro-Claisen condensation-like mechanism for the IpdAB-mediated hydrolysis of COCHEA-CoA. This study expands the range of known reactions catalyzed by the CoT superfamily and provides mechanistic insight into an important determinant of *Mtb* pathogenesis.**

steroid catabolism | coenzyme A transferase | carbon bond cleavage | tuberculosis | enzymology

The causative agent of tuberculosis, *Mycobacterium tuberculosis* (*Mtb*), was responsible for 1.8 million deaths in 2015, more than any other infectious agent worldwide (1). Current treatments are onerous and, with the emergence of drug-resistant strains such as MDR- and XDR-TB, novel therapeutics are urgently needed. The virulence and persistence of *Mtb*, an intracellular pathogen, is predicated on its ability to catabolize host-derived lipids, including cholesterol (2). Cholesterol catabolism is of burgeoning interest as disruption of a number of cholesterol catabolic genes generates attenuated or avirulent strains (3–5). More recently, a significant number of compounds selected for their ability to inhibit the intracellular growth of *Mtb* specifically inhibited cholesterol catabolism, suggesting that this process is a viable target for novel antituberculosis therapeutics (6). However, the function of many of the ∼80 cholesterol catabolic genes is poorly understood.

In *Mtb* and other mycolic acid-producing Actinobacteria, cholesterol catabolism can be described as three processes: (*i*) β-oxidation of the alkyl side chain, (*ii*) oxygenolytic cleavage of rings A and B, and (*iii*) β-oxidation of rings C and D. For the first two processes, many of the enzymatic steps have been well described (3, 7–9). We recently proposed a pathway for rings C and D degradation (10) beginning with 3aα-H-4α(3′-propanoate)-7aβ-methylhexahydro-1,5-indanedione (HIP). Briefly, HIP is thioesterified to HIP-CoA, then subjected to a series of β-oxidative reactions to yield HIEC-CoA, in which rings C and D are still intact. It was proposed that ring D is then hydrolyzed by EchA20, a member of the crotonase superfamily, to yield (*R*)-2-(2-carboxyethyl)-3-methyl-6-oxocyclohex-1-ene-1-carboxyl-CoA (COCHEA-CoA) (Fig. 1). Incubation of COCHEA-CoA with a CoA thiolase, FadA6, and IpdAB yielded a product presumed to be 4-methyl-5-oxo-octanedioyl-CoA (MOODA-CoA; Fig. 1) based on mass spectral data and the observation of MOODA accumulation in a Δ*fadE32* mutant (10). This last step indicates that either IpdAB or FadA6 is responsible for cleavage of steroid ring C. Further, Δ*ipdAB* mutants in each of *Mtb* and two other mycolic acid-producing Actinobacteria, *Mycobacterium smegmatis* and *Rhodococcus jostii* RHA1 (RHA1), accumulated COCHEA-CoA when incubated with cholesterol (10), suggesting that COCHEA-CoA is the physiological substrate of IpdAB. However, IpdAB has been annotated as a CoA transferase (CoT), sharing 27% amino acid sequence identity with glutaconate CoT (GCT) from *Acidaminococcus fermentans*, a heterotetrameric class I β-keto-CoT (11). It is unclear how a thiolase or a CoT might catalyze fission of a cyclohexene ring.

IpdAB has also been implicated in *Mtb* pathogenesis. Based on transposon mapping studies, *ipdAB* was predicted to be essential

Significance

All steroid-degrading bacteria utilize IpdAB, a predicted CoA transferase (CoT) that has been implicated in the hydrolysis of a carbon–carbon bond, an unprecedented reaction in CoTs. In *Mycobacterium tuberculosis*, IpdAB is required for degrading host cholesterol and virulence. We used a combination of X-ray crystallographic and biochemical studies to elucidate the mechanism of IpdAB. Superposition of the $IpdAB_{Mtb}$ active site with those of CoTs reveals distinct architectural features which, in conjunction with the biochemical data, indicate that IpdAB catalyzes a retro-Claisen-like ring-opening reaction. This reaction is unique for a member of the CoT superfamily. This study provides insights into bacterial steroid catabolism and facilitates the development of potential antituberculosis therapeutics targeting IpdAB.

Author contributions: A.M.C., S.D.W., N.W., L.J.W., N.C.J.S., and L.D.E. designed research; A.M.C., S.D.W., and N.W. performed research; A.M.C., S.D.W., N.W., L.J.W., N.C.J.S., and L.D.E. analyzed data; and A.M.C., S.D.W., L.J.W., N.C.J.S., and L.D.E. wrote the paper.

The authors declare no conflict of interest.

This article is a PNAS Direct Submission.

Data deposition: The atomic coordinates and structure factors have been deposited in the Protein Data Bank, www.wwpdb.org (PDB ID codes 6CO6, 6CO9, 6COJ, and 6CON).

[1]To whom correspondence should be addressed. Email: leltis@mail.ubc.ca.

This article contains supporting information online at www.pnas.org/lookup/suppl/doi:10.1073/pnas.1717015115/-/DCSupplemental.

Published online March 26, 2018.

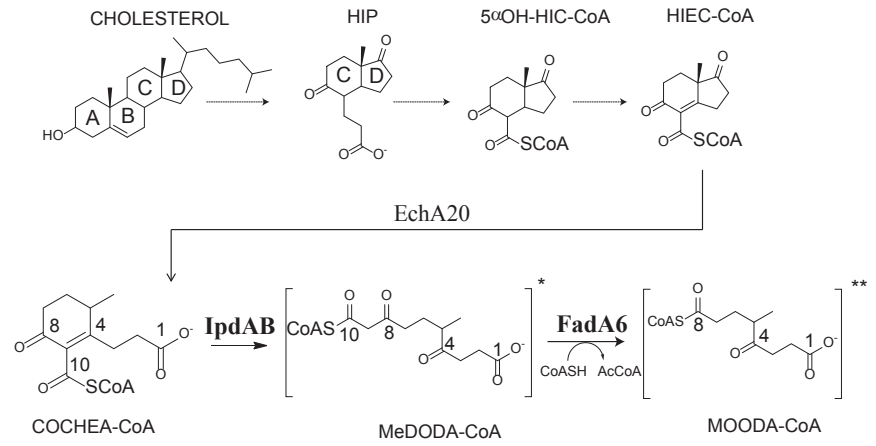

Fig. 1. Cholesterol rings C and D degradation in *Mtb*. R and R′ represent CoAS or O^-. Carbon numbering for COCHEA-CoA, MeDODA-CoA, and MOODA-CoA used within the text is displayed.

for the growth of *Mtb* in macrophages (12). Indeed, deletion mutants of *ipdAB* in *Mtb* had highly reduced growth rates in macrophages (10). Interestingly, an *ipdAB* mutant in the related horse pathogen *Rhodococcus equi* has been patented as a live vaccine for use in foals (13). Finally, Δ*ipdAB* mutants of *Mtb*, *M. smegmatis*, and RHA1 did not grow on cholesterol and were unable to grow on other carbon sources in the presence of cholesterol (10). This cholesterol-dependent toxicity correlated with highly depleted CoASH levels suggests that disruption of *ipdAB* results in CoA sequestration.

CoTs catalyze the reversible transfer of CoA from a CoA thioester to a free carboxylate (14, 15). Three classes of CoTs have been identified, the first two of which belong to the same superfamily. In class I CoTs, CoA is transferred from the acyl group of the donor substrate to a free carboxylate of an acceptor substrate, typically a small organic acid (11, 16, 17). These enzymes utilize a ping-pong mechanism in which a conserved glutamyl residue acts as a nucleophile to form a glutamyl-CoA intermediate before CoA transfer to the acceptor (Fig. S1*A*) (15, 18). In all class I CoTs characterized to date, the conserved glutamate occurs in the β subunit of the $\alpha_2\beta_2$ enzymes or the equivalent domain in the α_4 enzymes, toward the back of the active site (14, 16, 18, 19). Class II CoTs are subunits of the citrate and citramalate lyase complexes and catalyze the hydrolysis of small CoA thioesters using citrate or citramalate in a partial reaction analogous to class I CoTs (20, 21). Although class III CoTs belong to a different superfamily, they appear to utilize a mechanism similar to that of class II CoTs (22, 23).

Herein, we used a combination of X-ray crystallography, steady-state kinetics, directed mutagenesis, and isotopic labeling to characterize the reaction catalyzed by IpdAB from *Mtb* ($IpdAB_{Mtb}$) and RHA1 ($IpdAB_{RHA1}$). The data distinguish IpdAB from CoTs and indicate that IpdAB opens the last steroid ring of cholesterol by acting as a hydrolase. Overall, our study identifies a novel catalytic function within the CoT superfamily and provides important insights into a virulence determinant and potential target for novel antituberculosis therapeutics.

Results

Bioinformatic Analysis of IpdAB. To better understand the relationship of IpdAB to CoTs, we analyzed the phylogeny of IpdA and IpdB with the α and β subunits, respectively, of characterized class I and II CoTs. Sequence alignments were structure-guided and only sequences corresponding to the conserved core domains of the CoTs were used in the phylogenetic analysis to minimize bias resulting from insertions (Table S1). This analysis revealed that IpdA homologs from steroid-degrading bacteria formed a clade distinct from each of the three formed by the α subunits of the class I CoTs, class I β-keto-CoTs, and class II CoTs, respectively (Fig. 2). IpdAs clustered most closely with the heterotetrameric class I β-keto-CoTs and, within the IpdA clade, orthologs from actinobacteria (blue) and proteobacteria (green) formed subclades. Analysis of IpdBs with the CoT β subunits revealed similar relationships except that PcaI, the β subunit of

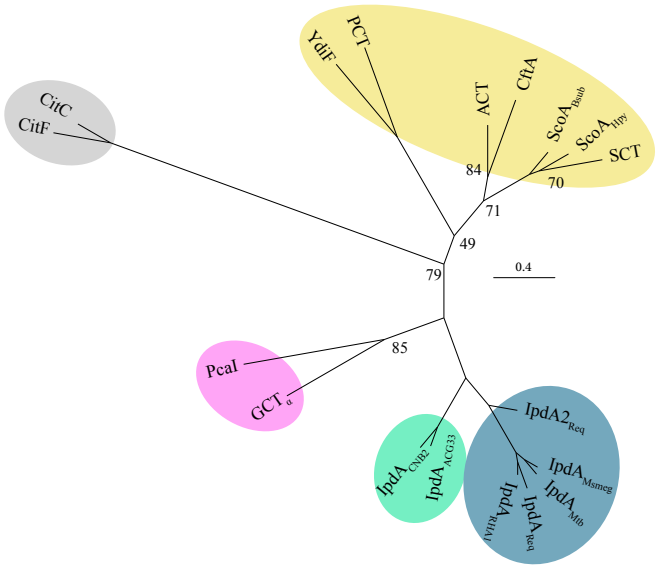

Fig. 2. Bioinformatic analysis of IpdAB and homologs. Phylogenetic tree displaying IpdA and α-subunits from class I and II CoTs. Shaded regions indicate gram-positive IpdA (blue), gram-negative IpdA (green), or class I β-keto-CoA (purple), class I (yellow) and class II (gray) CoTs. Proteins displayed are IpdA from *R. jostii* RHA1 ($IpdA_{RHA1}$), *R. equi* ($IpdA_{Req}$; $IpdA2_{Req}$), *M. smegmatis* ($IpdA_{Msmeg}$), *Mtb* ($IpdA_{Mtb}$), *Steroidobacter denitrificans* ($IpdA_{ACG33}$), and *Comamonas testosteroni CNB-2* ($IpdA_{CNB2}$); β-ketoadipyl-CoT from *Pseudomonas putida* (PcaI); glutaconate CoT from *A. fermentans* (GCT); citrate lyases from *Enterobacter aerogenes* (CitC) and *Clostridium argentinense* (CitF); butyrate-acetoacetate CoT from *Clostridium acetobutylicum* (CtfA); acetate CoTs from *E. coli* (ACT and YdiF); succinyl-CoTs from *Bacillus subtillus* ($ScoA_{Bsub}$), *Helicobacter pylori* ($ScoA_{Hpy}$), and pig heart (SCT); and propionyl-CoT from *Clostridium propionicum* (PCT). Additional information is available in *Supporting Information*. Numbers at tree nodes correspond to nonparametric bootstrap values from 100 maximum-likelihood calculations. Bootstrap values >90 are not displayed.

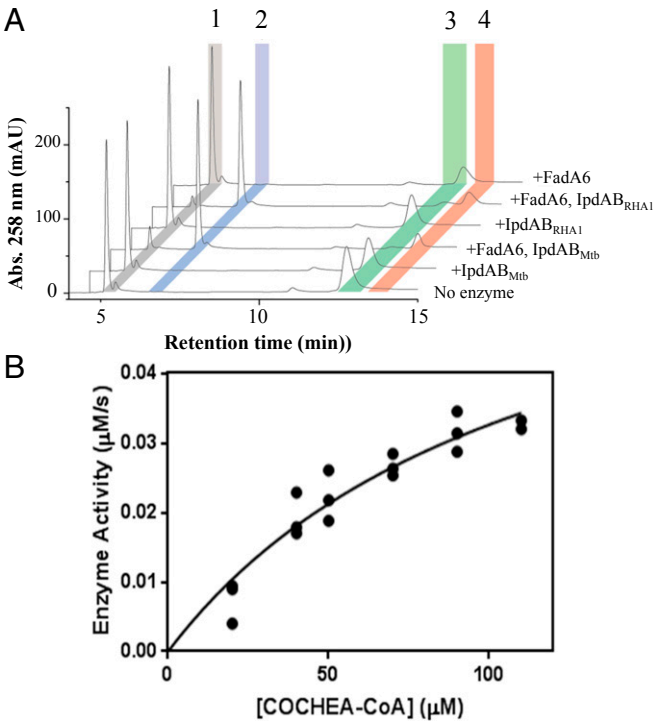

Fig. 3. In vitro activity of IpdAB. (*A*) HPLC trace of in vitro transformation of COCHEA-CoA with IpdAB and FadA6. Reaction conditions were 100 μM COCHEA-CoA, 1 μM IpdAB$_{RHA1}$/IpdAB$_{Mtb}$, 5 μM FadA6, and/or 125 μM CoASH (10 mM sodium phosphate, pH 8.0). Identified species correspond to CoASH (1), acetyl-CoA (2), COCHEA-CoA (3), and MOODA-CoA (4). (*B*) Steady-state analysis of IpdAB transformation of COCHEA-CoA [Hepes, pH 7.5, and1 mM $MgCl_2$ (I = 0.01 M) at 25 °C]. Curve indicates least-squares fit of Michaelis–Menten equation to the data.

the β-ketoadipate:succinyl-CoT PcaIJ, clustered differently than the α subunit, PcaJ (Fig. S1*B*).

Characterization of IpdAB. For biochemical and structural characterization of IpdAB, each of IpdAB$_{Mtb}$ and IpdAB$_{RHA1}$ (82% amino acid sequence identity) were overproduced and purified to apparent homogeneity using immobilized metal ion affinity chromatography (Fig. S2*A*). RHA1 was a better expression host than *Escherichia coli*. Further, IpdAB$_{RHA1}$ was produced to higher levels than IpdAB$_{Mtb}$ and was more stable once purified. Size-exclusion chromatography multiangle light scattering (SEC MALS) analyses revealed that IpdAB$_{RHA1}$ had a molecular weight of 109.7 ± 0.1 kDa, corresponding to an $\alpha_2\beta_2$ heterotetramer as reported for class I CoTs (16).

IpdAB Does Not Possess CoT Activity. All CoTs characterized to date catalyze the inter- or intramolecular transfer of CoA from a CoA thioester to a free carboxylate (14, 16). To test whether IpdAB$_{RHA1}$ had similar activity, the enzyme was incubated with a variety of CoA donors and small organic acids. HPLC analysis failed to detect the transfer of CoA from any of acetyl-CoA, propionyl-CoA and succinyl-CoA to acetate, propionate, or succinate. Additionally, IpdAB did not detectably catalyze the hydrolysis of CoA thioesters.

IpdAB Catalyzed the Efficient Transformation of COCHEA-CoA. It was previously reported that Δ*ipdAB* mutants accumulate COCHEA-CoA when incubated with cholesterol, and that incubation of COCHEA-CoA with IpdAB and a thiolase yielded a metabolite presumed to be MOODA-CoA (10). To extend this observation, the ability of IpdAB to transform COCHEA-CoA and other CoA thioesters was tested in vitro. In the presence of a thiolase, either FadA5 or FadA6 from *Mtb*, and CoASH, both IpdAB$_{Mtb}$ and IpdAB$_{RHA1}$ stoichiometrically transformed COCHEA-CoA into acetyl-CoA and a second CoA thioester of 952 *m/z*, consistent with MOODA-CoA (Fig. 3*A*). No compounds other than COCHEA-CoA, MOODA-CoA, acetyl-CoA, and CoASH were detected using liquid chromatography–MS (LC-MS). Neither IpdAB nor a thiolase alone detectably transformed COCHEA-CoA. Since IpdAB$_{Mtb}$ and IpdAB$_{RHA1}$ displayed similar activities, most of the subsequent studies were performed using the more stable ortholog, IpdAB$_{RHA1}$.

To evaluate the efficiency of the IpdAB reaction, we established a coupled assay with IpdAB$_{RHA1}$ and FadA6. We first evaluated the thiolytic activity of FadA6 toward β-keto CoA thioesters using acetoacetyl-CoA by following the decrease in absorbance at 310 nm from the acetoacetyl-CoA-Mg^{2+} enolate (Fig. S3*A*). The steady-state kinetic parameters indicated that FadA6 readily cleaves acetoacetyl-CoA (Table 1). In a coupled assay with IpdAB, the rate of COCHEA-CoA consumption, as measured spectrophotometrically by the decrease in absorbance at 252 nm, was limited by FadA6 at mole ratios below 400:1 (FadA6:IpdAB; Fig. S3*B*). The product of the IpdAB reaction was turned over by FadA6 at a rate of 0.014 ± 0.006 s^{-1}. In the presence of saturating amounts of FadA6, IpdAB$_{RHA1}$ had a relatively high specificity constant for COCHEA-CoA (k_{cat}/K_m = 5 × 10^4 $M^{-1}{\cdot}s^{-1}$; Fig. 3*B* and Table 1). Similar results were obtained using FadA5 instead of FadA6.

We definitively identified MOODA-CoA as the second CoA thioester produced in the enzymatic transformation of COCHEA-CoA using NMR. Comparison of the ^1H-^{13}C heteronuclear multiple bond correlation (HMBC) spectra of MOODA-CoA and MOODA revealed a ∼23 ppm increase in the chemical shift for carbon-8 (C-8) in MOODA-CoA compared with MOODA (Fig. S3*C*), establishing that the CoA moiety is attached at C-8 of MOODA. Given that all β-keto-CoA thiolases characterized to date, including FadA5 and FadA6, act on β-keto-CoA thioesters, the location of the CoA moiety on MOODA-CoA indicates that the substrate for FadA6 is 6-methyl-3,7-dioxodecanedioyl-CoA (MeDODA-CoA) (Fig. 1). Failure to observe this species in the absence of FadA6 may reflect that the equilibrium of the IpdAB-catalyzed reaction lies far to the left.

The Structural Fold of IpdAB Is Typical of Class I CoTs. To further characterize IpdAB, we solved the X-ray crystallographic structures of IpdAB$_{Mtb}$ and IpdAB$_{RHA1}$ to 2.1 and 1.7 Å resolution, respectively. The asymmetric units of the IpdAB$_{Mtb}$ and IpdAB$_{RHA1}$ crystals contained two $\alpha_2\beta_2$ heterotetramers and one αβ heterodimer, respectively. In the latter, the $\alpha_2\beta_2$ assembly was formed from two αβ protomers related by a twofold axis of symmetry in the crystal lattice (Fig. 4*A*), corroborating the SEC-MALS data. Ordered electron density for all residues in IpdAB$_{Mtb}$ was observed, except for the last two residues of IpdB$_{Mtb}$. For IpdAB$_{RHA1}$, ordered electron density was observed for all residues except for the N-terminal methionine of IpdA, which was removed with the affinity tag, and the first six residues of IpdB. Data collection and structure refinement statistics are presented in Table S2. The IpdAB$_{Mtb}$ and IpdAB$_{RHA1}$ heterotetramers are nearly identical

Table 1. Steady-state kinetic parameters

Enzyme	Substrate	k_{cat}, s^{-1}	K_m, μM	k_{cat}/K_m (×10^4 $M^{-1}{\cdot}s^{-1}$)
FadA6$_{Mtb}$*	Acetoacetyl-CoA	4.8 (0.8)	300 (100)	1.6 (0.8)
IpdAB$_{RHA1}$†	COCHEA-CoA	5.8 (0.8)	120 (40)	5 (2)

*Hepes, pH 7.5, and 10 mM $MgCl_2$ (I = 0.05 M), 25 °C.
†Hepes, pH 7.5, and 1 mM $MgCl_2$ (I = 0.01 M).

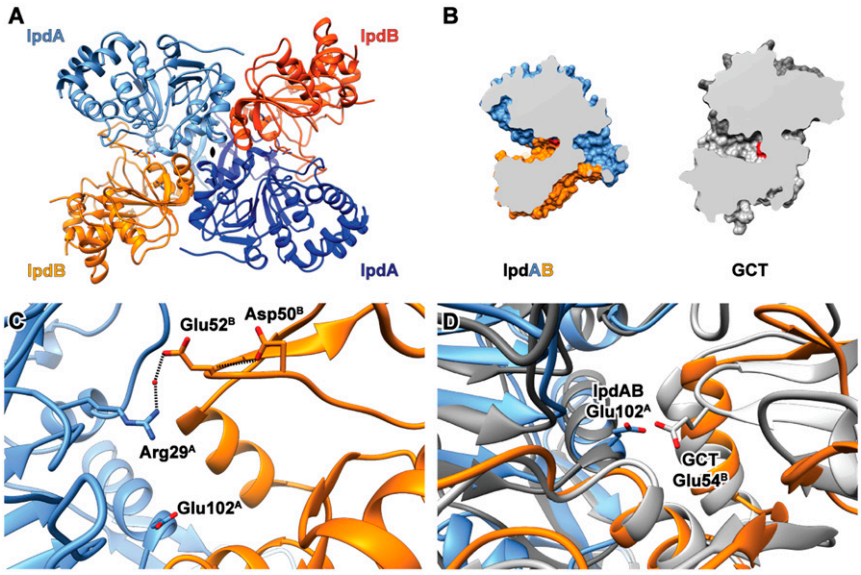

Fig. 4. Crystallographic structure of $IpdAB_{Mtb}$. (*A*) Heterotetrameric assembly of $IpdAB_{Mtb}$. IpdA and IpdB subunits are depicted as blue and orange ribbons, respectively. Active-site residues are shown as ball and stick models. (*B*) Comparison of substrate binding cleft topology for WT $IpdAB_{Mtb}$ (blue/orange) and a prototypical class I CoT enzyme GCT (gray; PDB ID code 1POI); catalytic residues are shown in red. (*C*) Location of potential candidates for the catalytic base in the β-subunit derived from structural alignments with other CoT enzymes are shown in ball and stick. (*D*) Superposition of the $IpdAB_{Mtb}$ (blue/orange) and GCT (gray) active sites showing the similar positioning of catalytic residues.

(rmsd of 0.43 Å on 486 common C_α) (Fig. S4*A*). The two most notable differences involve loops. The first involves a loop near the heterodimeric interface that is three residues shorter in $IpdAB_{RHA1}$ (Leu56-Glu72 and Phe62-Glu75in $IpdA_{Mtb}$ and $IpdA_{RHA1}$, respectively). The second involves a ∼2.7-Å outward rotation of the 10-residue loop between β-sheets 6 and 7 in $IpdA_{RHA1}$ relative to the C_α backbone of $IpdA_{Mtb}$ (Fig. S4*C*). The following discussion of the native structure is based on $IpdAB_{Mtb}$.

IpdAB possesses an αβ core fold similar to class I CoTs. More specifically, IpdA consists of a seven-stranded parallel β-sheet sandwiched between helices α_{1-4} on one side and α_{5-7} on the other. The core of IpdB is similar except that the β-sheet is six-stranded (with five parallel strands, one antiparallel) and is sandwiched between fewer helices (α_{1-2} and α_{5-6}, respectively). IpdA is further distinguished from IpdB by a 12-residue loop (consisting of Thr141-Thr153 in $IpdA_{Mtb}$) that overlaps the second IpdA subunit (denoted by $^{A'}$) and likely stabilizes the tetrameric assembly via two hydrogen bonds: one between $Tyr144^{A}$ (O^{η}) and $Gln138^{A'}$ (peptide N), and a second between $Gln138^{A}$ (N^{ε}) and $Pro143^{A'}$ (peptide O). Consistent with the phylogenetic analyses, the structural fold of IpdAB most closely resembles that of the $\alpha_2\beta_2$ class I CoT, GCT [Protein Data Bank (PDB) ID code 1POI] [rmsd of 2.45 Å on 409 C_α shared between $IpdAB_{Mtb}$ and GCT (Fig. 4*A*)].

IpdAB Has Distinct Active-Site Residues. Each $IpdAB_{Mtb}$ protomer harbors a single, large active-site pocket located at the interface between the two subunits. The pocket has an estimated volume of 1,775 $Å^3$ using CASTp 3.0 with a 1.8-Å probe (24) and lies between helix α_5 of IpdA, helices $\alpha_{3,4}$ of IpdB, and the β-sheet of IpdB. A channel of ∼30 Å in length projects out of the active site and follows the contours of the interface between the two subunits. The active-site pocket of $IpdAB_{Mtb}$ is similarly localized as in GCT, although the pocket of the latter is significantly smaller (650 $Å^3$, Fig. 4*B*). This difference is due in part to IpdB's active-site loop ($Thr49^{B}$ to $Gln54^{B}$) which, at five residues, is ∼16 residues shorter than that of GCT. The corresponding loop in GCT also harbors $Glu54^{\beta}$, the central catalytic nucleophile of class I CoTs (16). The shorter IpdB loop carries two distinct acidic residues, $Asp50^{B}$ and $Glu52^{B}$; however, the $Glu52^{B}$ ($Glu58^{B}$ in $IpdAB_{RHA1}$) carboxylate is directed away from the pocket and appears to stabilize the protomer by forming a water-mediated hydrogen bond and electrostatic interaction with the side chain of $Arg29^{A}$ (Fig. 4*C*). $Asp50^{B}$ also does not appear to be well-positioned for a catalytic role, appearing to contribute instead to the structural integrity of the active-site loop via a hydrogen bond to the peptide nitrogen of $Glu52^{B}$ (Fig. 4*C*). IpdAB has an additional acidic residue at the center of its active site, $Glu102^{A}$ ($Glu105^{A}$ in $IpdAB_{RHA1}$) (Fig. 4*D*). Inspection of sequence alignments used for the phylogenetic analyses revealed that $Glu102^{A}$ is conserved in IpdAB orthologs but not in class I CoTs (Fig. S1*C*). In contrast, the catalytic $Glu54^{\beta}$ of class I CoTs does not occur in any of the IpdAB orthologs.

Structure of IpdAB·COCHEA-CoA Complexes. To gain more insight into the function of IpdAB, structures of IpdAB·COCHEA-CoA complexes were obtained. In light of near identity of the respective active sites of $IpdAB_{RHA1}$ and $IpdAB_{Mtb}$, the former was employed due to the higher-order crystal quality. Structures of WT and $E105^{A}A$ in complex with COCHEA-CoA were solved to 1.6- and 1.4-Å resolution, respectively. The location of the thioester sulfur atom in the WT·COCHEA-CoA complex was further validated using anomalous scattering. Refinement data are summarized in Table S2. Structures of substrate-bound $IpdAB_{RHA1}$ were remarkably similar to the substrate-free $IpdAB_{RHA1}$ structure (rmsd of 0.21 Å on 462 common C_α atoms). The few notable differences include an rmsd displacement of the side-chain atoms of $Arg126^{B}$ and $Arg120^{B}$ by 3.3 and 1.0 Å, respectively, presumably to accommodate the substrate. With the exception of the acyl moiety in the active site and the substituted residue, the WT and $E105^{A}A$ substrate-bound structures were essentially indistinguishable (rmsd of 0.07 Å on 489 common C_α atoms). In both complexes, the substrate is bound in a channel between the subunits with the CoA adenine binding ∼20 Å away from $Glu105^{A}$. This is similar to what has been reported in class I CoTs (Fig. 5*A*) (25). For example, superposition of the IpdAB·COCHEA-CoA complexes with those of YdiF from *E. coli* (PDB ID code 2AHV) and pig heart SCOT (PDB ID code 3OXO) revealed that their

BIOCHEMISTRY

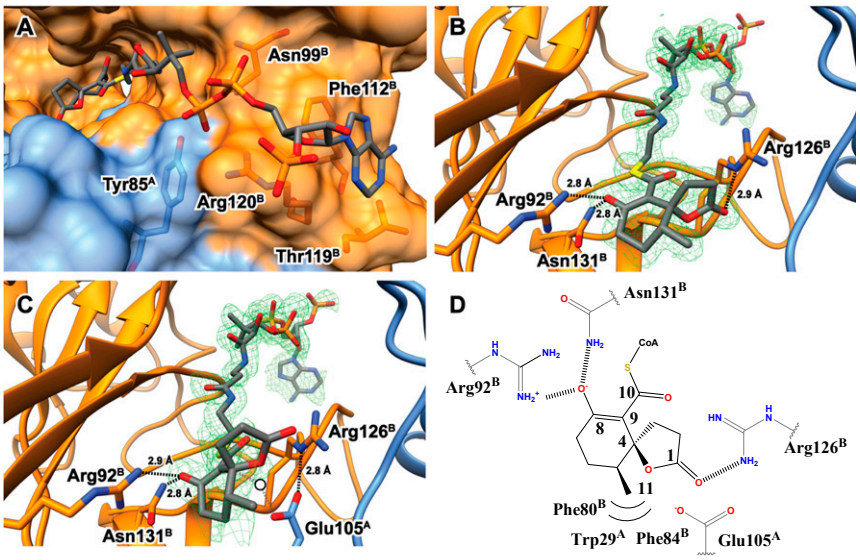

Fig. 5. Structure of IpdAB·COCHEA-CoA. (*A*) Lactonized COCHEA-CoA binds along a long cleft between IpdA (blue) and IpdB (orange). Residues proposed to be involved in binding of the CoA moiety are shown in ball and stick. (*B*) Active site of $IpdAB_{RHA1}$ $E105^{A}A$·COCHEA-CoA complex displaying putative catalytic residues in ball and stick. The mFo-DFc substrate omit map contoured at 3.0 σ is shown in green mesh. (*C*) Active site of the WT $IpdAB_{RHA1}$·COCHEA-CoA complex displaying putative catalytic residues in ball and stick. The mFo-DFc substrate omit map contoured at 3.0 σ is shown in green mesh. Potential position of catalytic water we suggest would be bound in the unlactonized form of substrate is represented by a white circle. (*D*) Diagram illustrating residues predicted to make contacts with the lactonized COCHEA-CoA in the $IpdAB_{RHA1}$ active site.

respective CoA sulfur atoms are within 1.2 Å of each other. Notable interactions between the CoA moiety and the protein include coordination of the diphosphate group by the side chains of $Arg120^{B}$, $Asn99^{B}$, and $Tyr85^{A}$; coordination of the ribose hydroxyl by $Arg147^{B}$; π–π stacking between the adenine group and $Phe112^{B}$; and coordination of the adenine amino group by $Thr119^{B}$ (Fig. 5*A*). In $IpdAB_{Mtb}$ these residues correspond to $Arg117^{B}$, $Asn96^{B}$, $Tyr82^{A}$, $Arg144^{B}$, $Phe109^{B}$, and $Thr116^{B}$, respectively (Fig. S1*C*). In addition, superposition of $IpdAB_{Mtb}$ with $IpdAB_{RHA1}$·COCHEA-CoA highlights the near identity of the active sites of these enzymes (Fig. S4*B*). Thus, all residues within 4.0 Å of COCHEA-CoA are conserved in $IpdAB_{Mtb}$. Indeed, the only pocket-lining residue that differs is Leu109 in $IpdB_{RHA1}$, which is Ile106 in $IpdB_{Mtb}$. However, this residue does not contact COCHEA-CoA. Interestingly, the side chain of $Arg123^{B}$ in $IpdAB_{Mtb}$ has the same rotamer as $Arg126^{B}$ in the $IpdAB_{RHA1}$·COCHEA-CoA and $E105^{A}A$·COCHEA-CoA complexes.

Electron density in the active site of the $E105^{A}A$·COCHEA-CoA complex clearly revealed a five-membered lactone ring generated from the cyclization of the C-1 carboxylate to C-4 (Fig. 5*B*). The cyclohexenone ring of the bound COCHEA-CoA is largely planar with the C-8 oxo and C-11 methyl group projecting ∼180° from each other. The lactone ring is orientated perpendicularly to the cyclohexanone ring such that C-4 is an (*S*) stereocenter. No electron density was observed corresponding to an (*R*) C-4 stereocenter (Fig. 5*B*). Torsional angles about C-4 deviate slightly from an optimal sp^3 hybridized center due to a slight bend of the lactone ring away from the C-11 methyl, resulting in angles of 104° and 110° for O-1/C-4/C-1 and O-1/C-4/C-5 bonds, respectively. Similarly, the C-8 oxo is bent slightly (Φ = 116°) toward $Arg92^{B}$ and forms hydrogen bonds with that residue (2.9 Å) and $Asn131^{B}$ (2.8 Å) (Fig. 5*B*). The C-11 methyl group sits in a hydrophobic pocket formed by $Phe80^{B}$, $Phe84^{B}$, $Val83^{B}$, and $Trp29^{A}$. Corresponding residues in $IpdAB_{Mtb}$ are provided in Fig. S1*C*.

Electron density in the active site of the WT $IpdAB_{RHA1}$·COCHEA-CoA complex was less resolved than in the $E105^{A}A$·COCHEA-CoA complex. However, additional residual density outside of the active site fit the CoA moiety well, suggesting that the substrate may bind in more than one conformation (Fig. 5*C*). Using a feature-enhanced map (26), density for the five-membered lactone observed in the $E105^{A}A$ structure could be clearly identified. No density for the C-1 carboxylate was observed, indicating that the unlactonized form of COCHEA-CoA was not present. Comparison of the lactonized COCHEA-CoA from the two structures illustrates distinct differences (Fig. 5 *B* and *C*). First, the cyclohexanone ring is not planar in the WT complex: The C-8 oxo is bent upward toward $Arg92^{B}$. Second, the C-8 oxo and C-10 thioester are also not planar, suggesting C-9 is sp^3 hybridized and protonated. Third, the lactone exhibits bond torsion between C-1/C-2/C-3 (Φ = 96°), deviating from the predicted 105°. Finally, the lactone in the WT structure is rotated ∼45° away from its location in the $E105^{A}A$ complex, presumably to avoid steric clash with $Glu105^{A}$. Interestingly, the O^{ε} of $Glu105^{A}$ forms a 2.8-Å hydrogen bond and electrostatic interaction with the N^{ε} of $Arg126^{B}$, positioning the $Glu105^{A}$ carboxylate directly under C-4 of COCHEA-CoA (Fig. 5*C*). In the absence of substrate lactonization, a water molecule could be accommodated between C-4 of COCHEA-CoA and $Glu105^{A}$ (Fig. 5*C*, white circle). Finally, in neither complex is there any evidence of an oxyanion hole to accommodate the CoA thioester oxo of the bound COCHEA-CoA. By contrast, an oxyanion hole appears to stabilize the thioester oxo in YdiF and SCOT (18).

Identification of Catalytically Essential Residues. The structural data indicate direct interactions between the acyl-moiety of COCHEA-CoA and each of the side chains of $Arg92^{B}$, $Glu105^{A}$, and $Arg126^{B}$ such that they may potentially activate the substrate during catalysis. $Glu58^{B}$, however, is located more than 12 Å away from the bound substrate and thus predicted not to play a direct role in catalysis. Importantly, these residues are all conserved in IpdABs (Fig. S1*C*). To test the catalytic relevance of these residues, each was substituted and the variants purified. CD spectroscopy and SEC MALS indicated that all variants had the same global secondary and tertiary structures as WT IpdAB (Fig. S2 *B* and *C*). The $E58^{B}A$ variant showed only a minor reduction in specific activity compared with WT, consistent with its localization and noncatalytic role. In contrast, the other variants ($E105A^{A}$, $E105D^{A}$, $R92M^{B}$, and $R126M^{B}$) had no detectable activity, consistent with these residues playing an essential role in catalysis (Table 2).

The IpdAB Reaction Mechanism Does Not Appear to Involve a Glutamyl-CoA Intermediate. In class I CoTs, the glutamyl-CoA intermediate has been trapped by incubating the reaction mixture with sodium borohydride ($NaBH_4$). This reduces the glutamyl-CoA intermediate to a thiohemiacetal, eventually yielding an alcohol and a loss in mass of 14 Da which may be observed using LC-MS (27). This also leads to the enzyme's irreversible inhibition. To test for the occurrence of a glutamyl-CoA intermediate in the turnover of IpdAB, we incubated a mixture of $IpdAB_{RHA1}$ and COCHEA-CoA with $NaBH_4$. LC-MS analysis of

Table 2. Specific activity of IpdAB variants

$IpdAB_{RHA1}$ variant	Relative activity, %
WT	100 (25)
$E58^{B}A$	80 (20)
$E105^{A}A$	<0.5
$E105^{A}D$	<0.5
$R126^{B}M$	<0.5
$R92^{B}M$	<0.5

Using 50 μM COCHEA-CoA, 50 μM CoASH, and 2 μM FadA6 [Hepes, pH 7.5, and 1 mM $MgCl_2$ (I = 0.01 M), 25 °C].

the incubated enzyme revealed no significant difference in mass of either the α (32,328 Da) or β (27,375 Da) subunits with respect to untreated IpdAB (Fig. S5*A*). Moreover, treatment with $NaBH_4$, either in the presence or absence of COCHEA-CoA, did not significantly reduce the specific activity of IpdAB following removal of the remaining sodium borohydride (Fig. S5*B*). These results strongly indicate that the IpdAB mechanism does not involve a glutamyl-CoA thioester intermediate.

Formation of a β-Keto Enolate in the $E105^{A}A$ Variant. The observation of the lactonized COCHEA-CoA in the $IpdAB_{RHA1}$ $E105^{A}A$ active site prompted us to test whether binding to IpdAB variants in solution perturbed the absorption spectrum of COCHEA-CoA. Titration of the $E105^{A}A$ variant with COCHEA-CoA yielded a stable yellow-colored species, ES_{yellow} (λ_{max} = 312 nm; Fig. 6*A*) consistent with an enolate. A dissociation constant (K_d) for COCHEA-CoA of 0.4 ± 0.2 μM was calculated from the titration data (Fig. 6*B*). This species was not observed in WT $IpdAB_{RHA1}$ or in either the $Arg92^{B}$ or $Arg126^{B}$ variants.

IpdAB Catalyzed Deuteration of COCHEA-CoA. Although $IpdAB_{RHA1}$ did not detectably transform COCHEA-CoA ($[M + H]^+$ = 976.196 Da) in the absence of FadA6, the observation of ES_{yellow} in the $E105^{A}A$ variant suggested that the enzyme might catalyze a reaction that is not detected using LC-MS, such as the rapid interchange between COCHEA-CoA and the ring-opened MeDODA (Fig. 1). We hypothesized that such a reaction would be detected by following deuterium incorporation into COCHEA-CoA from deuterium oxide (D_2O). Indeed, incubation of IpdAB and COCHEA-CoA in the presence of D_2O resulted in the formation of a new species with $[M + H]^+$ = 979.216 Da (Fig. 7*B*), consistent with deuteration at three positions. This species had the same HPLC retention time as COCHEA-CoA, consistent with the two compounds' being structurally identical. COCHEA-CoA was not deuterated in the absence of IpdAB (Fig. 7*B*), nor was the incorporated deuterium exchanged out when the 979 species was incubated in water in the absence of enzyme. The activity appears to be specific to COCHEA-CoA as $IpdAB_{RHA1}$ did not catalyze the deuteration of 5αOH-HIC-CoA or any other CoA thioester tested. LC-MS/MS with in-source fragmentation (MS^3) indicated that all three sites of deuteration were located on the acyl moiety. First, the characteristic 428 m/z fragment ion generated from CoA was observed in both species (Fig. 7*C*). Second, a diagnostic 181.0865 m/z fragment ion assigned as resulting from cleavage of the carboxy thioester in COCHEA-CoA was shifted to 184.1014 m/z in ^{2}[H]-COCHEA-CoA (Fig. 7*C*). Incubation of $IpdAB_{RHA1}$ and FadA6 with COCHEA-CoA and CoASH in buffered D_2O yielded $^2[H]_3$-MOODA-CoA (m/z = 955.2172 Da; Fig. S6*A*) and $^2[H]_3$-acetyl-CoA (m/z = 813.1544 Da; Fig. S6*B*). The $E105A^{A}$ variant did not catalyze deuteration of COCHEA-CoA (Fig. S6*C*).

To determine the rate and location of the IpdAB-catalyzed deuteration, the reaction was followed using NMR. A time-dependent decrease in the integration of the C-11 methyl doublet of COCHEA-CoA was observed (Fig. 7*D*), indicating exchange at C-5. This loss was not observed in the absence of IpdAB. The initial rate of deuteration at C-5 was calculated using Eq. **2** (Fig. 7*E*) at 40–50 s^{-1}, although the fit to data beyond 20 min was poor, likely due to the competition of ^{2}[H]-COCHEA-CoA for IpdAB. Monitoring the integration of a singlet from a methyl group in the CoA moiety confirmed that COCHEA-CoA did not significantly degrade during this experiment (Fig. 7*E*, gray). A concomitant decrease in the C-5 proton signal at 2.78 ppm was observed yielding highly similar results when used for measuring the rate of exchange. A time-dependent decrease in proton integration in the 2.4- to 2.6-ppm range was also observed, consistent with deuteration at C-3. However, LC-MS analysis of the COCHEA-CoA pre- and postincubation with $IpdAB_{RHA1}$ indicated that M + 1 ^{2}[H] was the most abundant species, suggesting that the rate of exchange at C-3 is significantly slower than at C-5.

^{18}O Is Not Incorporated into COCHEA-CoA or $IpdAB_{RHA1}$. To test whether the lactonized species observed in the IpdAB·COCHEA-CoA complexes is catalytically relevant, we incubated $IpdAB_{RHA1}$ and COCHEA-COA in the presence of >90% $H_2{}^{18}O$ and assayed for ^{18}O incorporation using LC-MS. More specifically, a retro-Claisen-like ring-opening reaction could be facilitated by hydrolysis of the lactone (reaction I, Fig. S6*D*), hydrolysis of a glutamyl ester (reaction II, Fig. S6*D*), or direct hydroxylation at C-4 (Fig. 8). Hydrolysis of the lactone in reaction I should result in ^{18}O incorporation at C-1 in the presence of $H_2{}^{18}O$. We did not detect any ^{18}O exchange into COCHEA-CoA using LC-MS (Fig. S6*E*). Moreover, intact protein LC-MS indicated that ^{18}O was not detectably incorporated into IpdAB as would be expected for the hydrolysis of the resulting acyl-enzyme ester linkage. Considering that carboxylates are not readily exchangeable (28, 29), the absence of ^{18}O incorporation into COCHEA-CoA or IpdAB indicates that hydroxylation occurs at C-4. Although these results preclude hydrolysis at the C-1 lactone, we cannot exclude the possibility that the lactonized COCHEA-CoA observed in the crystal structures has some other catalytic role.

As a positive control, incubation of $IpdAB_{RHA1}$, FadA6, COCHEA-CoA, and CoASH produced MOODA-CoA with a mass of 954.2 Da, consistent with the incorporation of ^{18}O at C-4 (Fig. S6*F*). Although ^{18}O incorporation into MOODA-CoA was observed (Fig. S6*F*), ^{16}O–^{18}O exchange occurred rapidly upon dilution into H_2O + 0.1% formic acid before LC-MS. Therefore, we were unable to conclude whether ^{18}O incorporation occurred from the hydrolysis of COCHEA-CoA or oxygen exchange at the C-4 ketone of MOODA-CoA after its production (30).

Discussion

This study provides evidence that IpdAB transforms COCHEA-CoA, thereby catalyzing the hydrolytic opening of the last ring in

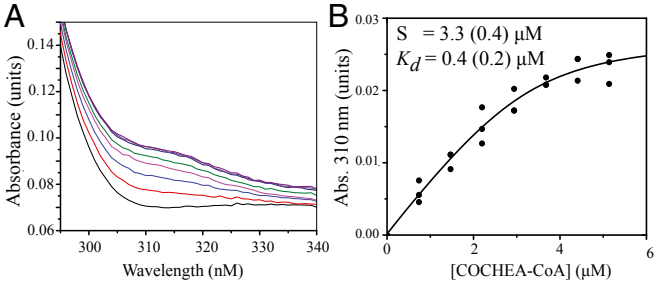

Fig. 6. The stabilization of an intermediate by IpdAB. (*A*) The UV-visible absorption spectra of 3.5 μM $IpdAB_{RHA1}$ $E105^{A}A$ (gray trace) titrated with up to 5 μM COCHEA-CoA (purple trace). The buffer was Hepes and 1 mM $MgCl_2$, pH 7.5 (I = 0.01 M). (*B*) Increase in absorbance at 310 nm of the $E105^{A}A$·COCHEA-CoA complex as a function of COCHEA-CoA concentration. The curve represents a fit of the quadratic binding equation to the data.

BIOCHEMISTRY

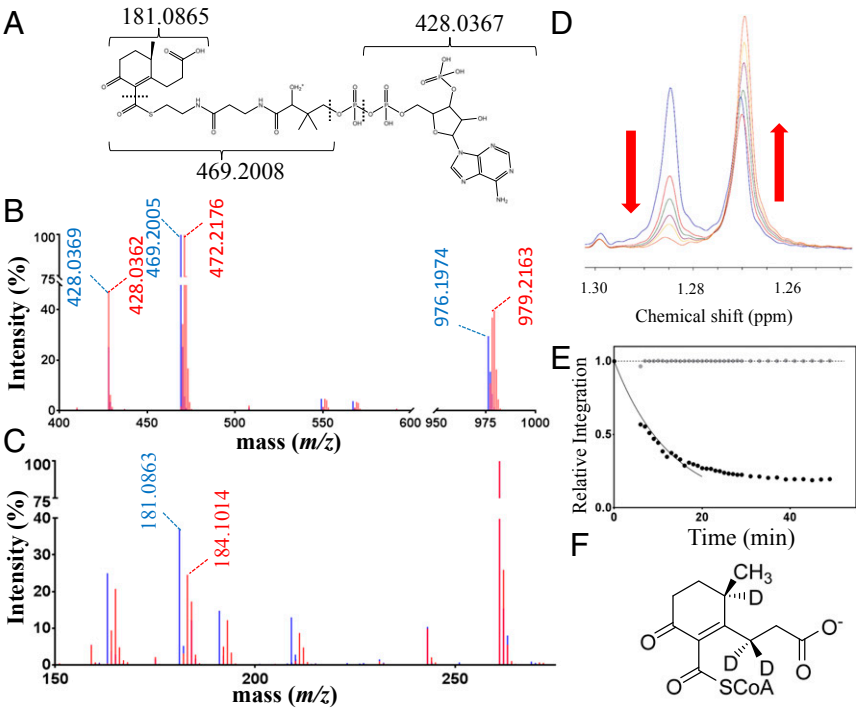

Fig. 7. IpdAB catalyzes proton exchange on COCHEA-CoA. (*A*) Diagram depicting predicted fragments from MS^3 on COCHEA-CoA. (*B*) LC-MS/MS mass spectra of COCHEA-CoA following incubation in D_2O with (red) and without (blue) $IpdAB_{RHA1}$. (*C*) LC-MS^3 mass spectra of COCHEA-CoA following incubation with (red) and without (blue) $IpdAB_{RHA1}$. (*D*) The ^{1}H-NMR spectra displaying the time-dependent decrease in the C-10 methyl doublet of COCHEA-CoA upon incubation of $IpdAB_{RHA1}$ in D_2O. The blue trace represents the spectrum before the addition of $IpdAB_{RHA1}$. The red, green, purple, yellow, and orange traces represent the spectra at 6, 11, 16, 21, and 52 min, respectively, after enzyme addition. (*E*) Time course displaying the relative decrease in proton integration for the C-9 methyl doublet (1.28 ppm; black dots) and the C-36 methyl group (0.75 ppm; gray dots) in the CoA moiety of COCHEA-CoA following addition of $IpdAB_{RHA1}$. Solid curve displays the best fit of Eq. **2** to the initial 20 min of data. Dotted line indicates relative intensity = 1.0. (*F*) Location of deuteration (D) on COCHEA-CoA as determined by NMR.

the bacterial catabolism of steroids. The data further indicate that this reaction does not involve CoA transfer despite IpdAB's striking similarity to class I CoTs. First, $IpdAB_{RHA1}$ did not catalyze the transfer of CoA from small acyl-CoA donors to small acids, a reaction typical of class I CoTs. Second, the IpdAB active site lacks key elements that are spatially conserved in CoTs including the catalytically essential glutamate and an oxyanion hole to accommodate the CoA thioester (18). Third, $NaBH_4$ did not detectably inhibit IpdAB, nor did it trap a glutamyl-CoA thioester intermediate. Finally, the position of the CoA in MOODA-CoA, the product of the $IpdAB_{RHA1}$/FadA6 reaction, indicates that the CoA is not transferred from one carbon to another before thiolysis. Therefore, our data support IpdAB as catalyzing the ring opening of COCHEA-CoA to MeDODA-CoA.

Based on the presented data, we propose a mechanism for IpdAB involving a retro-Claisen-like hydrolysis (Fig. 8). In this mechanism, binding of COCHEA-CoA to the $IpdAB_{Mtb}$ active site stabilizes the C-8 enolate resonant form of COCHEA-CoA via hydrogen bonding from the side chains of $Arg89^B$ and $Asn128^B$. A water, potentially activated by either $Glu102^A$ or the C-1 carboxylate, attacks at C-4, which is more electrophilic due to stabilization of the enolate. Tautomerization of the C-8 enolate protonates C-9. Deprotonation of the resulting C-4 hydroxyl yields an alkoxide anion, whose ketonization and concerted protonation at C-9 permits cleavage of the C-4/C-9 bond, opening ring C.

The proposed mechanism is supported by several lines of evidence. First, the $E105^AA_{RHA1}$ variant stabilizes a species whose spectrum is consistent with a CoA-enolate, as exemplified by the acetoacetyl-CoA-Mg^{2+} complex [λ_{max} = 310 nm (31)]. The structure of the $IpdAB_{RHA1}$·COCHEA-CoA complex suggests that $Arg89^B$ ($Arg92^B$ in $IpdAB_{Mtb}$) stabilizes the C-8 enolate. Second, deuteration at C-5 and C-3 is consistent with the increased electrophilicity of C-4. The failure of the $E105^AA_{RHA1}$ variant to catalyze deuteration of COCHEA-CoA indicates that deuteration occurs concerted with or after hydroxylation at C-4. Further, the rate of deuteration is an order of magnitude faster than COCHEA-CoA turnover and is thus not rate-limiting. Finally, the lack of ^{18}O incorporation at C-1 suggests that the lactonized COCHEA-CoA is not formed and directly hydrolyzed during catalysis, although the nucleophile could be activated by the C-1 carboxylate.

Several aspects of the mechanism remain to be elucidated. First, although the proposed mechanism posits $Glu102^A$ as the base that activates the nucleophile in $IpdAB_{Mtb}$, the structural data indicate that both this residue and the C-1 carboxylate may be positioned to activate water and/or deprotonate the C-4

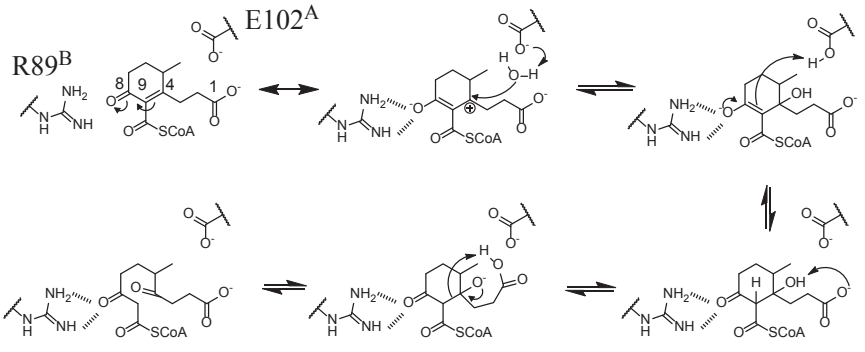

Fig. 8. Proposed mechanism of IpdAB. The respective catalytic roles of $Glu102^A$ and the substrate's C-1 carboxylate are unclear.

hydroxyl. Nevertheless, it is unclear whether the C-1 carboxylate is catalytically essential. Additional mechanistic studies involving the substrate were complicated due to limited quantities of COCHEA-CoA and the inability to directly observe its hydrolysis product despite various attempts to chemically trap MeDODA-CoA. Indeed, we cannot definitively exclude the possibility that IpdAB catalyzes an intramolecular CoA transfer from C-11 of COCHEA-CoA to C-11 in MeDODA-CoA. However, this is not supported by the results of the CoT studies and is thermodynamically unfavorable as formation of a carboxylic acid or ester would increase the pK_a of hydrogens at C-9, increasing the activation energy for C-4/C-9 hydrolysis.

The low turnover rate of FadA6 in the coupled reactions indicates that it may not be the physiological thiolase responsible for MOODA-CoA formation. Indeed, FadA5, which acts on the alkyl side chain of cholesterol (7), turned over MeDODA-CoA at the same rate as FadA6 in the coupled reaction. FadA6 may be required in the cleavage of 3′oxo- 5-OH-HIP-CoA to 5αOH-HIC-CoA, upstream of COCHEA-CoA in the HIP catabolic pathway (10). Overall, the enzyme acting on MeDODA-CoA has yet to be identified.

The hydrolytic cleavage of the cyclohexenone ring by IpdAB is similar to that catalyzed by Oah, a crotonase involved in the anaerobic degradation of benzoate in *Thauera aromatica* (32). Oah hydrolyzes the cyclohexene ring of 6-oxocyclohex-1-ene-1 carbonyl-CoA, a structural analog of COCHEA-CoA, by hydroxylating a double bond. Although the ensuing retro-Claisen opening of the cyclohexanone ring is comparable to that of IpdAB (Fig. 8), carbon–carbon cleavage occurs adjacent to the carbon double bond, yielding 3-oxopimeloyl-CoA, a β-keto CoA thioester analogous to MeDODA-CoA (32). Interestingly, the subsequent catabolism of 3-oxopimeloyl-CoA and MOODA-CoA are predicted to be similar (10, 33).

The phylogeny of *ipdAB* implies its divergent evolution from ancestral genes encoding a class I β-keto-CoT to facilitate the opening of steroid ring C. Interestingly, the degradation of HIP is predicted to yield methyl-β-ketoadipyl CoA (10). This metabolite is similar to β-ketoadipyl-CoA, the product of the class I β-keto-CoT PcaJI, involved in benzoate degradation (10, 34). HIP catabolism is not predicted to require a β-ketoadipate CoT-like PcaJI. However, the subsequent catabolic step in both pathways involves a thiolase and generates succinyl-CoA and either acetyl-CoA or propionyl-CoA (34). It is possible that duplication of the β-ketoadipate pathway may have facilitated the repurposing and divergent evolution of an ancestral PcaJI homolog to generate IpdAB.

Overall, our study of IpdAB provides a characterization of a mechanistically distinct member of the CoT family and provides insights into the evolution of steroid catabolism in bacteria. Due to its correlation with the pathogenesis of *Mtb* and other bacteria, IpdAB remains an intriguing target for therapeutics. In this respect, the substrate-binding and mechanistic features identified herein provide a basis for the specific targeting of IpdAB in the development of novel antituberculosis therapeutics.

Materials and Methods

Chemicals and Reagents. CoASH, NAD^+, FMN, sodium acetate, sodium propionate, sodium succinate, propionic anhydride, succinyl anhydride, acetoacetyl-CoA, and acetyl-CoA were purchased from Sigma-Aldrich. Restriction enzymes and T4 DNA ligase were purchased from New England Biolabs. Phusion DNA polymerase and Taq DNA ligase were purchased from Thermo Scientific. Oligonucleotides were purchased from Integrated DNA Technologies. The 5αOH-HIC was provided by Victor Snieckus, Queen's University, Kingston, Canada. All other reagents were of HPLC or analytical grade. Buffers and solvents were prepared as previously described (10).

Bioinformatic Analysis. Amino acid sequences of CoTs and IpdAB homologs were aligned using TCOFFEE EXPRESSO (35). For homomeric enzymes containing domains complementary to α and β subunits, the domains were treated separately. Phylogenetic trees were generated using the approximate likelihood-ratio test via PhyML on the phylogeny.fr server (36).

DNA Manipulation and Plasmid Construction. DNA was propagated, amplified, digested, ligated, and transformed using standard protocols (37). pTipR1IpdAB and pTipFadA6 were constructed as previously described (10). pTipHCol51, for $IpdAB_{Mtb}$ expression, was constructed by amplifying *rv3551-rv3552* from *Mtb* H37Rv genomic DNA using the sequences 5′-GCAATAGCATATGCATCACCATCACCATCACATCGAAGGTAGGGCATCGCCCGATAAACGAACCGCTC-3′ and 5-CGTAAG- CTTGGGAGAGGAGGCGGAACAATC-3. The *rv3551-rv3552* amplicon was digested with NdeI and HindIII then ligated into pTipQC2. Oligonucleotide-directed mutagenesis was performed using the QuikChange PCR protocol with slight modifications. Briefly, a single 5′ phosphorylated mutagenic DNA oligomer was annealed to pTipR1IpdAB then amplified using Phusion DNA polymerase. Taq DNA ligase was added to generate a single-stranded mutagenized plasmid. DpnI was used to remove template DNA and the remaining ssDNA was transformed into *E. coli* NovaBlue. pTipR1IpdAB variants $E58^BA$, $E105^AA$, $E105^AD$, $R92^BM$, and $R126^BM$ were generated using the following respective oligonucleotides (substituted nucleotides are underlined): 5′-pCTGATCACCGACGGTGCGGCCCTGATCTTCGCG-3′, 5′-pGTCCGCGAAATGGACGCGGGCATGGTCAAGTGC-3′, 5′-pGTCCGCGAAATGGACGACGG-CATGGTCAAGTGC-3′, 5′-pTCGCCTCCGGCCGGATGCACGTGGTGATGG-3′, and 5′-pCAGATG-TTCGGCGTCATGGGCGCACCCGGCAAC-3′. The nucleotide sequence of variants was confirmed.

Production of COCHEA-CoA. COCHEA-CoA was produced enzymatically from 5αOH-HIC-CoA as previously described (10) with the following variations. Following synthesis of 5αOH-HIC-CoA, the reaction mixture was onto 100 mg prepacked 2-(2-pyridyl)ethyl-functionalized silica (54127-U; Supelco), washed with acetonitrile:isopropanol:water:acetic acid (9:3:4:4 vol:vol:vol:vol) to remove unreacted precursors, then eluted in 20 mM ammonium acetate (pH 7.0) in 80% methanol. Methanol was removed under nitrogen. Four micromoles of 5αOH-HIC-CoA were added to a mixture containing $IpdC_{DOC21}$ (5 μM), IpdF (5 μM), $EchA20_{RHA1}$ (5 μM), $IpdAB_{RHA1}$ (1 μM), 1 mM NAD^+, and 10 μM FMN in 50 mM sodium phosphate, pH 8.0. The reaction mixture was incubated at 30 °C until completion as determined using HPLC (~3 h). Proteins were precipitated using methanol and the reaction mixture was lyophilized overnight then suspended in 500 μL water. COCHEA-CoA (t_R = 6.1 min) was purified using an HP1100 series HPLC (Agilent Technologies) equipped with a Luna 3u PFP (2) 50- × 4.6-mm column (Phenomenex) operated at 1 $mL{\cdot}min^{-1}$ and separated over a gradient of 20.0–30.2% methanol (90%) in 100 mM ammonium acetate, pH 4.5. HPLC- purified fractions of COCHEA-CoA were pooled, lyophilized, and then suspended in 400 μL water. To desalt, COCHEA-CoA was loaded onto an HPLC equipped with the PFP (2) column, washed for 2 min with water + 0.1% acetic acid, then eluted using 100% methanol. Typical mole yields of 25% were observed from racemic 5αOH-HIC-CoA.

Protein Production and Purification. $IpdC_{DOC21}$, $IpdF_{Mtb}$, $EchA20_{RHA1}$, $FadA6_{Mtb}$, and $FadA5_{Mtb}$ were purified as previously described (10, 38). $IpdAB_{Mtb}$, $IpdAB_{RHA1}$, and variants were produced using RHA1 as a host strain as previously described (10) with the following modifications. Following nickel affinity chromatography, IpdAB and its variants were dialyzed overnight against 25 mM Hepes, pH 7.5, and 50 mM NaCl then concentrated to ~5 $mg{\cdot}mL^{-1}$ to which 1:1,000 (mol:mol) α-thrombin was added and allowed to digest at room temperature for up to 20 h until complete as determined using SDS/PAGE. Digested IpdAB was loaded onto a 10/100 MonoQ anionic exchange column (GE Healthcare) and purified using an AKTA Purifier (GE Healthcare) operated at 2 $mL{\cdot}min^{-1}$ in 25 mM Hepes, pH 7, using a gradient of 150–400 mM NaCl. Eluted IpdAB (at a conductance of ~32 and 36 mS/cm for $IpdAB_{Mtb}$ and $IpdAB_{RHA1}$, respectively) was exchanged into 25 mM Hepes, pH 7.5, and 50 mM NaCl and concentrated using a 10-kDa molecular weight cutoff Amicon centrifugation unit (Millipore). Enzyme was flash-frozen in liquid nitrogen as beads and stored at −80 °C until further use. Typically, 5 and 80 mg of $IpdAB_{Mtb}$ and $IpdAB_{RHA1}$, respectively, were produced from 1-L culture of RHA1.

Protein Characterization. CD spectra were recorded at room temperature using a Jasco model J-810 spectropolarimeter. Far-UV CD spectra (190–250 nm) were recorded using a 1-mm quartz cuvette containing 3 μM protein in 10 mM sodium phosphate, pH 8.0. Cuvettes were continuously purged with nitrogen during spectra collection. Spectra were recorded in triplicate and averaged. SEC-MALS data were obtained using a HPLC 1260 Infinity LC (Agilent Technologies) coupled to a Superdex 200 5/150 column (GE Healthcare). Data were collected using a miniDAWN TREOS multiangle static light-scattering device and an Optilab T-rEX refractive index detector (Wyatt Technologies). Samples of 25 μL containing 0.5 $mg{\cdot}mL^{-1}$ protein were analyzed. The HPLC was operated at 0.25 mL/min in 25 mM Hepes, pH 7.5,

and 50 mM NaCl. Molecular weights of complexes were calculated using the ASTRA6 program (Wyatt Technologies). Protein concentrations were measured using the bicinchoninic acid protein assay with BSA as a standard.

Crystallization. Crystals of $IpdAB_{Mtb}$ and $IpdAB_{RHA1}$, respectively, were obtained using the sitting-drop vapor diffusion method at room temperature. $IpdAB_{Mtb}$ crystals were grown using 1 μL of protein solution (20–25 mg·mL^{-1}) mixed with an equal volume of reservoir solution (25% PEG 3350 and 0.5 M magnesium formate). $IpdAB_{RHA1}$ crystals were grown using 1 μL of protein solution (10 mg·mL^{-1}) mixed with an equal volume of reservoir solution (1.9 M ammonium sulfate and 0.2 M sodium potassium tartrate), crystals were observed within 7 d for WT and 60 d for the E105^{A}A mutant. To obtain substrate-bound crystals, 5 μL of ∼10 mM COCHEA-CoA in 2.4 M ammonium sulfate and 0.2 M sodium potassium tartrate was added directly to protein crystals in the drop and allowed to soak for 24–72 h at room temperature.

Crystallographic Analysis and Refinement. Single $IpdAB_{RHA1}$ and $IpdAB_{Mtb}$ crystals were looped and flash-frozen in liquid N_2 without additional cryoprotectant. Diffraction data for $IpdAB_{Mtb}$, $IpdAB_{RHA1}$ and the $IpdAB_{RHA1}$ E105^{A}A COCHEA-CoA complex were collected at Beamline 08B1-1 at the Canadian Light Source. Diffraction data for $IpdAB_{RHA1}$·COCHEA-CoA complex were collected at Beamline 5.0.2 at the Advanced Light Source. All $IpdAB_{RHA1}$ data were processed using Xia2 (39), XDS (40), and Aimless (41). $IpdAB_{Mtb}$ data were processed using Xia2 (39), DIALS (42), and Aimless (41). The $IpdAB_{RHA1}$ structure was solved by molecular replacement using Phaser (43) with a search model based on the backbone atoms of coordinate set PDB ID code 1POI. Both WT and E105^{A}A·COCHEA-CoA complex structures were solved by molecular replacement using Phaser with the $IpdAB_{RHA1}$ structure as a search model. Iterative cycles of model-building and refinement were performed with Coot (44) and Phenix (45). For the $IpdAB_{RHA1}$ WT·COCHEA-CoA complex, a feature-enhanced map (26) was used to guide the placement of ligand in the active site. $IpdAB_{Mtb}$ crystals appeared to belong to space group $P2_12_12_1$, although subsequent structure solution with molecular replacement failed to give a clear solution. Analysis of the diffraction data revealed the crystals were pseudomerohedrally twinned with a twin fraction of 20–30%. Reprocessing of the data in space group $P2_1$ enabled structure determination. The structure was solved by molecular replacement using Phaser (43) with a Chainsaw- (46) generated search model based on the $IpdAB_{RHA1}$ structure. Iterative cycles of model building and refinement were performed with Coot and Refmac5 and refinement was carried out both with and without amplitude-based twin refinement strategies as implemented in Refmac5 (statistics for both shown in Table S2). The solution was frequently validated using an approach incorporating debiasing [phenix.dynamics (45), reset of B-factors, omission of residues] to ensure the final refined model was in good agreement with the experimental data. Coordinates and structure factors have been deposited in the PDB (ID codes 6CO6, 6CO9, 6COJ, and 6CON). A summary of the data and refinement statistics is presented in Table S2.

IpdAB Activity. The transformation of various acyl-CoAs was performed in 100 μL 10 mM sodium phosphate, pH 8.0, containing 1 μM $IpdAB_{RHA1}$, 100 μM COCHEA-CoA, 125 μM CoASH, and, as appropriate, 5 μM FadA6. Reactions were incubated at room temperature for 1 h and terminated with the addition of 200 μL MeOH (0.5% acetic acid). To test CoT activity, the reactions contained either 100 μM acetyl-CoA, propionyl-CoA, succinyl-CoA, COCHEA-CoA, or MOODA-CoA 100 μM each of acetate, propionate, succinate, and MOODA. Reaction products were analyzed using a HP1100 Series HPLC attached to a 4.6- × 50-mm Luna 3u PFP (2) column operated at 1 mL·min^{-1}. A gradient of 0–90% methanol in 100 mM ammonium acetate, pH 4.5, over 20 min was employed to separate CoA thioesters as previously described (10).

Steady-State Kinetic Characterization. Steady-state kinetic parameters were evaluated using spectrophotometric assays recorded on a Cary 5K UV-Vis-NIR spectrophotometer (Agilent Technologies). The FadA6-catalyzed thiolysis of acetoacetyl-CoA was determined using 0.1 μM FadA6, 100 μM CoASH, and 50–600 μM acetoacetyl-CoA in 200 μL Hepes, pH 7.5, and 10 mM $MgCl_2$ (I = 0.05 M) at 25 °C by following the decrease in absorbance at 303 nm due to loss of the acetoacetyl-CoA-Mg^{2+} enolate [ε = 16.9 mM^{-1}·cm^{-1} (7)] as previously described (38). The IpdAB-catalyzed hydrolysis of COCHEA-CoA was followed using a coupled reaction with FadA6 by following the consumption of COCHEA-CoA at 252 nm (ε = 17.2 mM^{-1}·cm^{-1}). Reactions were performed in 200 μL Hepes, pH 7.5, and 1 mM $MgCl_2$ (I = 0.01 M) at 25 °C containing 50 μM CoASH, 5 μM FadA6, 0.01 μM IpdAB, and 20–110 μM COCHEA-CoA. The specific activity of $IpdAB_{RHA1}$ variants was determined using 2 μM FadA6, 50 μM COCHEA-CoA, 50 μM CoASH, and 0.01–3.5 μM IpdAB variant. The extinction coefficient of COCHEA-CoA was empirically derived by measuring the decrease in absorbance at 252 nm upon complete conversion to MOODA-CoA [$\varepsilon_{310\ nm}$ = 11.9 mM^{-1}·cm^{-1} (10)]. Steady-state kinetic parameters were determined by least fit squares fitting of the Michaelis–Menten equation to the data using the GraphPad analysis software.

Structure Assignment for MOODA-CoA. To determine the structure of MOODA-CoA using NMR, 1 μmol COCHEA-CoA was incubated with 2 μM IpdAB, 10 μM FadA6, and 2 μmol CoASH in 10 mM sodium phosphate, pH 8.0, at room temperature. Upon completion, the proteins were removed using methanol and the reactions were lyophilized overnight. The resulting residue was suspended and dried twice in 500 μL deuterated methanol then suspended in 400 μL D_2O. The ^{1}H-NMR, ^{1}H-^{1}H COSY, ^{1}H-^{1}H total correlation spectroscopy, and ^{1}H-^{13}C HMBC spectra were collected on a Bruker 600-MHz spectrophotometer. The sample contained MOODA-CoA (1.0 mM), acetyl-CoA (1.3 mM), and CoASH (1.3 mM). NMR data were analyzed using the Academic TopSpin 3.5 (Bruker). Spectra of MOODA-CoA were compared with those previously recorded for MOODA (10).

Attempts to Observe Acyl-Enzyme Intermediates. Fifty micromolar COCHEA-CoA and 50 μM $IpdAB_{RHA1}$ were incubated in 50 μL of 10 mM sodium phosphate, pH 8.0, for 5 min, then sodium borohydride was added to a final concentration of 20 mM. After an additional 30 min of incubation, samples were thoroughly desalted and exchanged into water using a 10-kDa Centricon centrifugation unit (EMD Millipore). The molecular weight of intact protein samples was determined using a Waters Xevo G2 qTOF operated by the University of British Columbia Proteomic Core Facility. The specific activity toward COCHEA-CoA was tested for the desalted $IpdAB_{RHA1}$ as described above for the IpdAB variants.

K_d Determination for IpdAB E105^{A}A. The K_d of $IpdAB_{RHA1}$ E105^{A}A for COCHEA-CoA was determined by following the increase in absorbance at 310 nm upon formation of the complex. $IpdAB_{RHA1}$ E105^{A}A (5 μM) was titrated with 0–5.2 μM COCHEA-CoA in 200 μL Hepes, pH 7.5, and 1 mM $MgCl_2$ (I = 0.01 M) at 25 °C. The reference cuvette contained 200 μL Hepes, pH 7.5, and 1 mM $MgCl_2$ (I = 0.01 M) at 25 °C. Difference spectra were recorded after each addition of substrate to the two cuvettes. Data used for calculation represent the difference between titrations of COCHEA-CoA into IpdAB E105^{A}A or assay buffer alone. The instrument was blanked using the assay buffer. Steady-state kinetic parameters and K_ds were determined by least fit squares fitting of the Michaelis–Menten equation or quadratic binding equation (Eq. **1**) to their respective datasets using the GraphPad analysis software:

$$A_{310} = A_o + A_{max}\left(\frac{(E+S+K_d) \pm \sqrt{(E+S+K_d)^2 - 4ES}}{2S}\right). \quad [1]$$

Deuterium Incorporation into COCHEA-CoA. One-hundred-micromolar COCHEA-CoA was incubated for 30 min with and without $IpdAB_{RHA1}$ in 50 μL of 10 mM sodium phosphate, pH 8.0, prepared in D_2O. Reactions were terminated by 5 μL of acetic acid. Samples were centrifuged to remove precipitated protein then filtered 0.45 μm, diluted 1:49 in water and analyzed by LC-MS/MS and/or LC-MS^3.

Proton–Deuterium Exchange NMR Experiments. Proton–deuterium exchange experiments were performed in 400 μL 10 mM sodium phosphate, pH 8.0, on a Bruker 500-MHz spectrophotometer. Before use, $IpdAB_{RHA1}$ was exchanged into 10 mM sodium phosphate, pH 8.0, in D_2O using a Nanosep 10K Centrifugal Device (PALL Life Sciences). The ^{1}H-NMR spectra of 1.6 mM COCHEA-CoA were recorded before and after addition of 50 nM IpdAB every minute for 45 min. A delay of 5 min occurred between the addition of IpdAB and the first recorded spectra. Aliquots of the reaction at the start and end of the experiments were analyzed by LC-MS to confirm incorporation of deuterium into COCHEA-CoA. A time-course plot of relative proton integration was generated by normalizing each proton integration with the C-37 methyl group in the CoA moiety. The initial rate of deuterium exchange at C-9 of COCHEA-CoA was calculated using a linear regression of Eq. **2** to the first 10 min of data performed by GraphPad. [S] was calculated using Eq. **3**, where $[S]_o$, $H_a(t)$ and $H_{0.91}(t)$ represent the initial substrate concentration and the integration of proton (a) or C-37 at time t, respectively:

$$\frac{d[S]}{dt} \sim -k[S][E] \quad [2]$$

$$[S] = [S]_o \frac{H_a(t)}{H_{0.91}(t)}. \quad [3]$$

^{18}O Labeling of COCHEA-CoA, MOODA-CoA, and IpdAB. One-hundred-micromolar COCHEA-CoA was incubated with and without 5 μM $IpdAB_{RHA1}$ (or 5 μM IpdAB, 20 μM FadA6, and 125 μM CoASH in MOODA-CoA experiments) in 50 μL of 10 mM sodium phosphate, pH 8.0, repaired in 97% $^{18}[O]H_2O$ (Sigma-Aldrich) for 15 min at room temperature. Reactions were terminated with the addition of 2 μL acetic acid or 200 μL methanol. Samples were ultracentrifuged (16,000 × *g*, 5 min) to remove protein, filtered through 0.45-μm polytetrafluoroethylene, then immediately frozen in liquid nitrogen and stored at −80 °C until analysis by LC-MS/MS. To look at ^{18}O labeling of IpdAB, the reactions were performed as described above; however, no acetic acid or methanol was added. IpdAB was desalted into water using a 10K centrifugation unit (Millipore) then subjected to intact protein MS as described above.

MS. Mass spectra were recorded using a Qstar mass spectrometer (Agilent Technologies) coupled to an HP 1100 series HPLC (Agilent Technologies) equipped with a 50- × 0.3-mm C18 (2) column operated at in positive ion mode (ion spray voltage = +5,500 V, ion source temperature = 350 °C). CoA thioesters were eluted using a gradient of 100 mM ammonium formate, pH 3.5, into acetonitrile + 0.1% formic acid at a flow rate of 4 μL·min^{-1}. High-resolution MS^3 of CoA thioesters were analyzed on a Bruker Impact-II Q-ToF equipped with a 150- × 0.25-mm Luna 3 μm PFP (2) (Phenomenex) column as previously described (10). CoA thioesters were eluted using a gradient of 100 mM ammonium acetate in 2% methanol and 20 mM ammonium acetate in 98% methanol. Mass spectrometers were calibrated daily.

ACKNOWLEDGMENTS. This work was supported by Canadian Institutes for Health Research (CIHR) Operating Grant MOP-1333647 (L.D.E.); operating grants from CIHR and the Howard Hughes International Senior Scholar program (to N.C.J.S.); and graduate scholarship funding from the Natural Sciences and Engineering Research Council of Canada (NSERC) and CIHR (to S.D.W. and A.M.C., respectively). N.C.J.S. is a Tier I Canada Research Chair in Antibiotic Discovery.

1. WHO (2016) Global tuberculosis report 2016 (WHO, Geneva).
2. Russell DG, Barry CE, 3rd, Flynn JL (2010) Tuberculosis: What we don't know can, and does, hurt us. *Science* 328:852–856.
3. Yam KC, et al. (2009) Studies of a ring-cleaving dioxygenase illuminate the role of cholesterol metabolism in the pathogenesis of *Mycobacterium tuberculosis*. *PLoS Pathog* 5:e1000344.
4. Hu Y, et al. (2010) 3-Ketosteroid 9alpha-hydroxylase is an essential factor in the pathogenesis of *Mycobacterium tuberculosis*. *Mol Microbiol* 75:107–121.
5. Pandey AK, Sassetti CM (2008) Mycobacterial persistence requires the utilization of host cholesterol. *Proc Natl Acad Sci USA* 105:4376–4380.
6. VanderVen BC, et al. (2015) Novel inhibitors of cholesterol degradation in *Mycobacterium tuberculosis* reveal how the bacterium's metabolism is constrained by the intracellular environment. *PLoS Pathog* 11:e1004679.
7. Nesbitt NM, et al. (2010) A thiolase of *Mycobacterium tuberculosis* is required for virulence and production of androstenedione and androstadienedione from cholesterol. *Infect Immun* 78:275–282.
8. Capyk JK, D'Angelo I, Strynadka NC, Eltis LD (2009) Characterization of 3-ketosteroid 9α-hydroxylase, a Rieske oxygenase in the cholesterol degradation pathway of *Mycobacterium tuberculosis*. *J Biol Chem* 284:9937–9946.
9. Capyk JK, Casabon I, Gruninger R, Strynadka NC, Eltis LD (2011) Activity of 3-ketosteroid 9α-hydroxylase (KshAB) indicates cholesterol side chain and ring degradation occur simultaneously in *Mycobacterium tuberculosis*. *J Biol Chem* 286:40717–40724.
10. Crowe AM, et al. (2017) Catabolism of the last two steroid rings in *Mycobacterium tuberculosis* and other bacteria. *MBio* 8:e00321-17.
11. Buckel W, Dorn U, Semmler R (1981) Glutaconate CoA-transferase from *Acidaminococcus fermentans*. *Eur J Biochem* 118:315–321.
12. Rengarajan J, Bloom BR, Rubin EJ (2005) Genome-wide requirements for *Mycobacterium tuberculosis* adaptation and survival in macrophages. *Proc Natl Acad Sci USA* 102:8327–8332.
13. van der Geize R, Grommen AW, Hessels GI, Jacobs AA, Dijkhuizen L (2011) The steroid catabolic pathway of the intracellular pathogen *Rhodococcus equi* is important for pathogenesis and a target for vaccine development. *PLoS Pathog* 7:e1002181.
14. Heider J (2001) A new family of CoA-transferases. *FEBS Lett* 509:345–349.
15. White H, Jencks WP (1976) Mechanism and specificity of succinyl-CoA:3-ketoacid coenzyme A transferase. *J Biol Chem* 251:1688–1699.
16. Jacob U, et al. (1997) Glutaconate CoA-transferase from *Acidaminococcus fermentans*: The crystal structure reveals homology with other CoA-transferases. *Structure* 5:415–426.
17. Selmer T, Buckel W (1999) Oxygen exchange between acetate and the catalytic glutamate residue in glutaconate CoA-transferase from *Acidaminococcus fermentans*. Implications for the mechanism of CoA-ester hydrolysis. *J Biol Chem* 274:20772–20778.
18. Rangarajan ES, et al. (2005) Crystallographic trapping of the glutamyl-CoA thioester intermediate of family I CoA transferases. *J Biol Chem* 280:42919–42928.
19. Murphy JR, Mullins EA, Kappock TJ (2016) Functional dissection of the bipartite active site of the class I coenzyme A (CoA)-transferase succinyl-CoA:acetate CoA-transferase. *Front Chem* 4:23.
20. Dimroth P, Loyal R, Eggerer H (1977) Characterization of the isolated transferase subunit of citrate lyase as a CoA-transferase. Evidence against a covalent enzyme-substrate intermediate. *Eur J Biochem* 80:479–488.
21. Buckel W, Bobi A (1976) The enzyme complex citramalate lyase from *Clostridium tetanomorphum*. *Eur J Biochem* 64:255–262.
22. Berthold CL, Toyota CG, Richards NG, Lindqvist Y (2008) Reinvestigation of the catalytic mechanism of formyl-CoA transferase, a class III CoA-transferase. *J Biol Chem* 283:6519–6529.
23. Leutwein C, Heider J (2001) Succinyl-CoA:(R)-benzylsuccinate CoA-transferase: An enzyme of the anaerobic toluene catabolic pathway in denitrifying bacteria. *J Bacteriol* 183:4288–4295.
24. Dundas J, et al. (2006) CASTp: Computed atlas of surface topography of proteins with structural and topographical mapping of functionally annotated residues. *Nucleic Acids Res* 34:W116–W118.
25. Fraser ME, Hayakawa K, Brown WD (2010) Catalytic role of the conformational change in succinyl-CoA:3-oxoacid CoA transferase on binding CoA. *Biochemistry* 49: 10319–10328.
26. Afonine PV, et al. (2015) FEM: Feature-enhanced map. *Acta Crystallogr D Biol Crystallogr* 71:646–666.
27. Hersh LB, Jencks WP (1967) Isolation of an enzyme-coenzyme A intermediate from succinyl coenzyme A-acetoacetate coenzyme A transferase. *J Biol Chem* 242:339–340.
28. Niles R, et al. (2009) Acid-catalyzed oxygen-18 labeling of peptides. *Anal Chem* 81: 2804–2809.
29. Redington RL (1976) Kinetics of oxygen-18 exchange between carboxylic acids and water. *J Phys Chem* 80:229–235.
30. Byrn M, Calvin M (1966) Oxygen-18 exchange reactions of aldehydes and ketones. *J Am Chem Soc* 88:1916–1922.
31. Middleton B (1973) The oxoacyl-coenzyme A thiolases of animal tissues. *Biochem J* 132:717–730.
32. Laempe D, Jahn M, Fuchs G (1999) 6-Hydroxycyclohex-1-ene-1-carbonyl-CoA dehydrogenase and 6-oxocyclohex-1-ene-1-carbonyl-CoA hydrolase, enzymes of the benzoyl-CoA pathway of anaerobic aromatic metabolism in the denitrifying bacterium *Thauera aromatica*. *Eur J Biochem* 263:420–429.
33. Harwood CS, Burchhardt G, Herrmann H, Fuchs G (1998) Anaerobic metabolism of aromatic compounds via the benzoyl-CoA pathway. *FEMS Microbiol Rev* 22:439–458.
34. Wells T, Jr, Ragauskas AJ (2012) Biotechnological opportunities with the β-ketoadipate pathway. *Trends Biotechnol* 30:627–637.
35. Armougom F, et al. (2006) Expresso: Automatic incorporation of structural information in multiple sequence alignments using 3D-coffee. *Nucleic Acids Res* 34: W604–W608.
36. Dereeper A, et al. (2008) Phylogeny.fr: Robust phylogenetic analysis for the non-specialist. *Nucleic Acids Res* 36:W465–W469.
37. Sambrook J, Russell DW (2001) *Molecular Cloning: A Laboratory Manual* (Cold Spring Harbor Lab Press, Cold Spring Harbor, NY), 3rd Ed.
38. Schaefer CM, et al. (2015) FadA5 a thiolase from Mycobacterium tuberculosis: A steroid-binding pocket reveals the potential for drug development against tuberculosis. *Structure* 23:21–33.
39. Winter G (2010) xia2: An expert system for macromolecular crystallography data reduction. *J Appl Crystallogr* 43:186–190.
40. Kabsch W (2010) XDS. *Acta Crystallogr D Biol Crystallogr* 66:125–132.
41. Evans PR, Murshudov GN (2013) How good are my data and what is the resolution? *Acta Crystallogr D Biol Crystallogr* 69:1204–1214.
42. Pugalenthi G, Archunan G, Sowdhamini R (2005) DIAL: A web-based server for the automatic identification of structural domains in proteins. *Nucleic Acids Res* 33: W130–W132.
43. McCoy AJ, et al. (2007) Phaser crystallographic software. *J Appl Cryst* 40:658–674.
44. Emsley P, Cowtan K (2004) Coot: Model-building tools for molecular graphics. *Acta Crystallogr D Biol Crystallogr* 60:2126–2132.
45. Adams PD, et al. (2010) PHENIX: A comprehensive Python-based system for macromolecular structure solution. *Acta Crystallogr D Biol Crystallogr* 66:213–221.
46. Stein N (2008) CHAINSAW: A program for mutating pdb files used as templates in molecular replacement. *J Appl Crystallogr* 41:641–643.